THE JOURNAL OF PHYSICAL CHEMISTRY Letters

Letter

pubs.acs.org/JPCL

The Role of Broken Symmetry in Solvation of a Spherical Cavity in Classical and Quantum Water Models

Richard C. Remsing,*[,†,∥] Marcel D. Baer,[§] Gregory K. Schenter,[§] Christopher J. Mundy,*[,§] and John D. Weeks*[,†,‡]

[†]Institute for Physical Science and Technology and [‡]Department of Chemistry and Biochemistry, University of Maryland, College Park, College Park, Maryland 20742, United States

[§]Physical Sciences Division, Pacific Northwest National Laboratory, Richland, Washington 99354, United States

Supporting Information

ABSTRACT: Insertion of a hard sphere cavity in liquid water breaks translational symmetry and generates an electrostatic potential difference between the region near the cavity and the bulk. Here, we clarify the physical interpretation of this potential and its calculation. We also show that the electrostatic potential in the center of small, medium, and large cavities depends very sensitively on the form of the assumed molecular interactions for different classical simple point-charge models and quantum mechanical DFT-based interaction potentials, as reflected in their description of donor and acceptor hydrogen bonds near the cavity. These differences can significantly affect the magnitude of the scalar electrostatic potential. We argue that the result of these studies will have direct consequences toward our understanding of the thermodynamics of ion solvation through the cavity charging process.

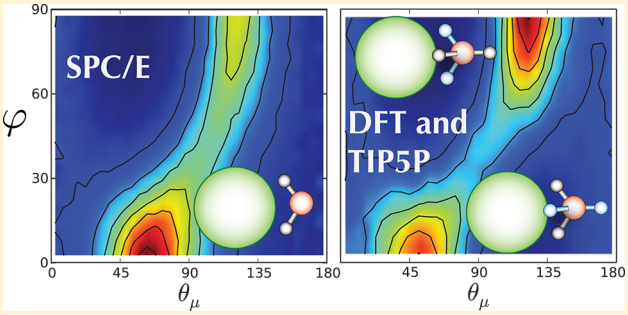

SECTION: Molecular Structure, Quantum Chemistry, and General Theory

The solvation of ions in water presents many conceptual and computational challenges to current models of ion and water interactions. The solvation free energy is usually described using a two step process: (i) the formation of a cavity in water that accommodates the neutral ion core along with its associated ion−water dispersion interactions and (ii) the additional free energy resulting from charging the core to the full charge of the ion. The simplest Born model treats water outside the cavity as a continuum dielectric that responds linearly to the inserted charge, and predicts that the resulting electrostatic free energy contribution is independent of the sign of the charge.[1−8] This disagrees with experiment, and workers have long recognized that nonlinear electrostatic effects induced by the initial insertion of the uncharged ion core must be taken into account.[1,2,4−7,9−14] These nonlinearities arise from the molecular nature of the system, since steric effects arising from inserting even a neutral ion core can strongly perturb local water molecules, affecting the number and arrangements of local hydrogen bonds and orientations of molecular dipoles and other multipoles.

The fixed cavity or ion core itself breaks the translational symmetry of the bulk solvent and induces molecular scale interfaces between the solute and solvent. The nonuniform charge density induced by a neutral solute can be generally characterized as a locally broken charge symmetry, and will typically generate an electrostatic potential difference between the region near the solute and in the bulk solvent. Accounting for this potential difference as the solute itself is further charged represents an important correction to the Born theory.[1,2,5,6]

However, water and other molecular solvents can also exhibit broken angular symmetry from nonspherical molecular cores and asymmetric intramolecular charge distributions. Using quantum chemistry results, Agmon has suggested that regions with a net effective positive charge in a water molecule are localized near the distinct hydrogen sites, while the associated negative charge is smeared nearly uniformly along a "negativity track" between the classical lone pair sites.[15] Broken angular symmetry from any source would give rise to differences between donor and acceptor hydrogen bonds even in bulk water, and this should have more dramatic effects on the molecular scale interfaces and asymmetric charge densities induced by solvation of neutral and charged solutes.

In this paper we study the structural and electrostatic consequences of the various broken symmetries that arise from inserting the simplest model of an uncharged ion core, a hard sphere solute, or cavity of varying radius R_C, into water as described by two classical water models, SPC/E[16] and TIP5P,[17] and by state of the art quantum density functional theory (DFT) calculations. We consider a state near the triple point at

Received: May 27, 2014
Accepted: July 11, 2014
Published: July 11, 2014

liquid−vapor coexistence with T = 300 K. As we will show, the broken symmetries from hard sphere solvation generate special configurations that are particularly sensitive to small differences between neighboring donor and acceptor hydrogen bonds and to local variations in the induced charge density.

Hydrogen bonds in almost all classical water models arise from "frustrated charge pairing", where an effective positive charge on a donor hydrogen site of one molecule is strongly attracted to a negatively charged acceptor site on a neighboring molecule.[18,19] This strong attractive force is opposed by the overlap of the repulsive Lennard-Jones (LJ) cores centered on the oxygen sites and the presence of other hydrogen sites in the acceptor molecule. Indeed, the thermodynamic stability of these classical models requires that the effective point charges be embedded inside harshly repulsive molecular cores that prevent a positive charge in one molecule from approaching too closely to a negative charge in another.

The classical SPC/E and TIP5P models differ qualitatively in their treatment of donor and acceptor hydrogen bonds. Both models place positive effective point charges on explicit hydrogen sites displaced tetrahedrally outward from the central oxygen site. In the TIP5P model, two negative point charges are similarly located on explicit "lone-pair" sites on the other side of the oxygen site, while in the SPC/E model, a single negative point charge is placed on the central oxygen site. Because of the more symmetric treatment of positive and negative charges, we would expect much smaller differences in properties of donor and acceptor hydrogen bonds in TIP5P water as compared to SPC/E water. Moreover, charge pairing to distinct negative sites in TIP5P should also yield hydrogen bonds with reduced angular fluctuations when compared to those in SPC/E and related three- and four-site water models like TIP4P, where all the negative charge is placed on a single site located much further inside the LJ core. This permits greater flexibility in accepting hydrogen bonds from neighboring molecules and effectively generates a classical version of the negativity track discussed by Agmon.[15]

The negativity track may be more apparent if we consider a "smeared" SPC/E model (SSPC/E) where the oxygen point charge in each molecule is replaced by a spherically symmetric charged shell with the same total charge and a radius equal to the hydrogen distance. Equivalently, we can add to the charges in the original model a spherically symmetric neutral charge distribution with a positive point charge equal in magnitude to the original oxygen charge placed at the oxygen center and a neutralizing negative charge smeared on a spherical shell with radius equal to the hydrogen distance. By Gauss' law, a test charge located outside the smeared shells in any configuration of SSPC/E or SPC/E water will experience exactly the same net force.[20] Thus, most relevant structural and thermodynamic properties of the two models are the same, as will be discussed in more detail later.

However, the smeared charge distributions clearly do change *intramolecular* Coulomb energies, but such terms are constant in rigid classical models and are usually ignored. One notable exception, however, is the value of the mean electrostatic or "Bethe" potential ϕ_B of a translationally invariant bulk liquid phase relative to a bulk vacuum of zero density.[21−23] For the rigid point charge models considered here, this is proportional to the density times the negative of the trace of the primitive molecular quadrupole tensor as given by

$$\mathrm{Tr}\{Q_{\mathrm{mol}}\} = \frac{1}{2}\sum_{\gamma=1}^{\Gamma} q_\gamma r_\gamma^2 \tag{1}$$

where for a given choice of molecular center, r_γ is the distance to the effective charge q_γ and the sum is over the Γ charged sites in the molecule.[24,25] The added spherically symmetric neutral charge distributions change only this molecular trace and hence ϕ_B with no modification of the molecular dipole or the usual traceless quadrupole moments.[20] By construction in the SSPC/E model, the trace is set equal to zero using the oxygen site as the molecular center, while it is positive in the SPC/E model. There has been much discussion in the literature about the possible role of the Bethe potential in ionic solvation, see, e.g., reviews by Hunenberger and Reif[26] and Lin et al.[27] and references therein, and our consideration of smeared models below should help clarify this point.

In this paper we focus on the physically relevant differences in the classical SPC/E and TIP5P models, and in quantum DFT descriptions of *intermolecular* interactions by accurately determining the solvent response to a hard sphere of varying radius. Although DFT has been used to study hydrophobic solvation for small molecular solutes in the past,[28] the use of hard spheres with different radii affords an unbiased comparison between the various water models that will ultimately lead to an assessment of their accuracy for understanding solvation.

Differences between the water models are most evident in their description of donor and acceptor hydrogen bonds. The donor/acceptor asymmetries are not easily seen in common measures of interfacial structure like the nonuniform density (see Supporting Information (SI)), but they are manifested in the orientational structure of water around solutes, and therefore the manner in which the hydrogen bond network is maintained in the interfacial region. The orientation of a water molecule relative to the solute can be uniquely defined by two angular coordinates:[29] θ_μ and φ. The first of which is the angle formed by the vector between the water oxygen and the center of the solute, $\vec{r}_{OS}$, and the dipole moment vector of the water molecule, $\vec{\mu}$, where $\vec{r}_{OS}$ points in the direction of the solute. The coordinate φ is the angle made by the projection of $\vec{r}_{OS}$ onto a local xy-plane and the local x-axis, which is normal to the H−O−H plane.

Joint probability distributions $P(\theta_\mu\varphi)$ are shown in Figure 1 for water molecules within 1 Å of the surface of a hard sphere with a radius of R_C = 4 Å, for the classical SPC/E and TIP5P models, as well as DFT results obtained with both the revPBE and BLYP functionals. This solute size is near the upper end of the small length scale regime of hydrophobic interactions, where the hydrogen bond network is basically maintained around the solute.[19,30−35] There are two dominant orientations; both correspond to a water molecule pointing one H-bonding group directly toward the bulk while the other three H-bonds continue around the solute. In the case of SPC/E water (Figure 1a), pointing the donor hydrogen sites around the solute is preferred, such that an acceptor group is pointed into the bulk, indicated by the large peak at low φ labeled B. However, the orientation obtained upon interchange of donor/acceptor groups, orientation $\tilde{B}$, is much less populated. Pointing acceptor groups outward provides more opportunities for hydrogen bonding between the first and second shells in SPC/E water. However, this asymmetry is nearly absent in the TIP5P model as in shown Figure 1b, as would be expected from the nearly

dx.doi.org/10.1021/jz501067w | J. Phys. Chem. Lett. 2014, 5, 2767−2774

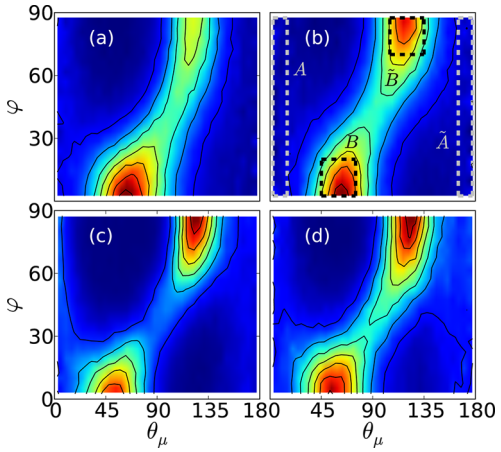

Figure 1. Joint probability distributions $P(\theta_\mu\varphi)$ calculated for molecules within 1 Å of the surface of the solute with R_C = 4 Å for the classical (a) SPC/E and (b) TIP5P water models, as well as the corresponding distributions obtained from DFT-based simulations using the (c) BLYP and (d) revPBE functionals. Red indicates high probability, while blue corresponds to low probability. The specific orientations discussed in the text and in Figure 2 are indicated in panel b by the dashed regions.

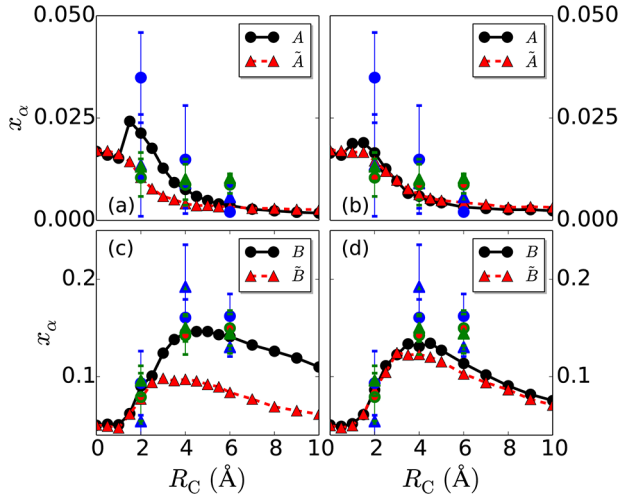

Figure 2. Solute size dependence of the fractions of orientations α and $\tilde{\alpha}$ in (a,c) SPC/E and (b,d) TIP5P water models for (a,b) $\alpha = A$ and (c,d) $\alpha = B$. The data for BLYP (blue) and revPBE (green) is replicated and superimposed on both the SPC/E and TIP5P data for direct comparison. The error bars for the DFT data represent standard deviations.

symmetric treatment of donor and acceptor sites. Interestingly, the results obtained from both sets of DFT simulations are also consistent with a nearly symmetric representation depicted in panels c (BLYP) and d (revPBE) of Figure 1, in stark contrast to what is expected from previous *ab initio* studies that support the negativity track picture discussed by Agmon and others.[15]

Hydrogen bond configurations and the associated nonuniform charge density near the inserted solute have very interesting behavior as the solute radius is varied,[19,30−35] with the most dramatic change occurring at a crossover radius between volume and area scaling of the hydrophobic free energy $R_X \approx 0.5$ nm.[33] Hydrogen bonds must be broken to accommodate larger solutes, and the resulting molecular interface resembles the liquid−vapor interface of water. Both SPC/E and TIP5P give qualitatively similar descriptions of this enthalpically driven length scale transition and of the interfacial and electrostatic properties of large solutes, but just below the transition differences in the arrangements of donor and acceptor bonds discussed above can play a key role.

We classify these arrangements through the fraction of hydration shell waters $x_\alpha(R_C)$ in orientation α as a function of solute size in Figure 2, where the orientations are defined in Figure 1. Orientation $\tilde{\alpha}$ corresponds to interchanging the lone pair and hydrogen sites of orientation α. Panels a and c of Figure 2 show that significant asymmetries between α and $\tilde{\alpha}$ persist in SPC/E water for all solute sizes under study. In contrast, panels b and d of Figure 2 depict that TIP5P water is much more symmetric with regard to interchange of donor and acceptor sites (α and $\tilde{\alpha}$) for all R_C; any small asymmetries are commensurate with the slight differences between the lone pair and hydrogen sites. Note that the dominant orientational populations display a peak in the vicinity of R_X for both models, supporting the idea that the qualitative features of the length-scale transition are captured by both potentials, while the specific details involving donor/acceptor asymmetry near the crossover differ.

Also shown in Figure 2 are the BLYP and revPBE data. Although there are clear convergence issues, especially for the 2 Å sphere size, the data suggests more symmetric populations of donor/acceptor sites in agreement with the TIP5P water model. The smaller error bars in revPBE are likely due to the initial conditions; they were taken from converged BLYP calculations. In contrast, the BLYP calculations were started from equilibrated SPC/E configurations, and the strong movement away from the donor/acceptor asymmetry that is present in the SPC/E water model depicted in Figures 1 and 2 gives us confidence in our conclusions reported in this study.

The donor/acceptor angular asymmetries and the corresponding broken charge symmetries discussed here clearly also affect the electrostatic potential in the vicinity of the water-solute interface and inside the solute. Related electrostatic effects will play an even more important role when the solute is fully charged to model an ion. We will discuss the effects of charging the solute and the relation to previous work elsewhere and focus here on electrostatic properties of the uncharged hard sphere.

To make contact with previous work.[4,6,7,12,13,36] we consider a slab geometry with explicit planar liquid−vapor interfaces and measure the electrostatic potential relative to that of the dilute vapor phase. More precisely we can insert a hard wall in the vapor phase and take the potential zero as that of the electrostatic vacuum inside the wall, and will ignore the small potential change between the hard wall and the dilute vapor. Since there is complete drying at coexistence with water vapor at the hard wall interface,[35] this is an excellent approximation. (This hard wall setup will also allow us to use this same interfacial framework and potential zero at densities other than the coexistence density as will be discussed elsewhere.)

We now consider the change in the electrostatic potential when a test charge is moved from this hard wall vacuum into and through the liquid−vapor interface and the liquid phase, and then through the molecular scale interface surrounding a cavity of radius R_C located in the liquid phase and into the cavity center, as schematically depicted in Figure 3. Subtle differences in orientational structure can lead to dramatic changes in the value of the mean electrostatic potential at the center of the cavity Φ^{HW}, termed the cavity potential herein. The HW superscript indicates the presence of the hard wall

dx.doi.org/10.1021/jz501067w | J. Phys. Chem. Lett. 2014, 5, 2767−2774

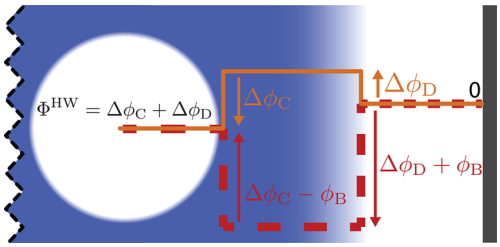

Figure 3. A schematic of a cavity immersed in a slab of water near the length-scale transition, with a liquid−vapor interface and hard wall far from the solute on the right, illustrated by the gradient in color. In our simulations, there are also symmetrically placed interfaces on the left, but this portion of the system is omitted from the schematic, as indicated by the dashed black line. Dashed lines indicate the electrostatic potential of the classical SPC/E model of water, while solid lines are indicative of the potential for a smeared variant of the same model, which has zero Bethe potential.

liquid−vapor interface and potential zero far from the solute, necessary because charging free energies rigorously consider moving a test charge from vacuum to the center of the cavity. As we will see, the cavity potential depends only on the same physically relevant *intermolecular* Coulomb forces that contribute directly to interfacial solvent structure, independent of possible smearing that would change the value of the Bethe potential.

In principle, the electrostatic potential in a particular configuration $\bar{\mathbf{R}}$ of the nonuniform solvent at a fixed observation point $\mathbf{r}$ is

$$\phi(\mathbf{r};\bar{\mathbf{R}}) = \int d\mathbf{r}' \frac{\rho^q(\mathbf{r}';\bar{\mathbf{R}})}{|\mathbf{r}-\mathbf{r}'|} \tag{2}$$

Here $\rho^q(\mathbf{r};\bar{\mathbf{R}})$ is the total charge density at $\mathbf{r}$ in configuration $\bar{\mathbf{R}}$, the ensemble average of which is $\rho^q(\mathbf{r}) = \langle\rho^q(\mathbf{r};\bar{\mathbf{R}})\rangle$. Similarly, $\phi(\mathbf{r};\bar{\mathbf{R}})$ is the scalar potential at position, such that the ensemble averaged electrostatic potential is $\phi(\mathbf{r}) = \langle\phi(\mathbf{r};\bar{\mathbf{R}})\rangle$. However, care must be exercised in taking ensemble averages in eq 2.

Since an idealized test charge is not affected by the nonelectrostatic potentials defining the classical molecular cores, the ensemble averaged potential $\phi(\mathbf{r})$ at a general point $\mathbf{r}$ in the solvent can have contributions from certain configurations where the test charge at $\mathbf{r}$ is inside a molecular core. Indeed such configurations can lead to a nonzero Bethe potential in eq 1 for a uniform system even though the ensemble averaged charge density $\rho^q(\mathbf{r}) = 0$ for all $\mathbf{r}$. However, as stressed by ref 23, results from typical experimental probes and standard measures of solvation free energies should not depend on these intramolecular terms.

This is particularly clear for the cavity potential $\Phi^{HW} \equiv \phi(0)$, where the observation point is inside the fixed cavity. Because of the shielding LJ cores between different water molecules and the presence of the hard sphere cavity, only intermolecular Coulomb interactions are sampled in all physically relevant configurations in eq 2. Thus, smeared and unsmeared models must give identical results for Φ^{HW}, independent of the value of the Bethe potential.

The numerical determination of the cavity potential has been a source of much confusion throughout the literature. A wide range of estimates that are inconsistent even in the sign of the potential have been reported.[1,2,4,6,11,14,37−43] Here we show how these results can be consistently interpreted by removal of the model-dependent Bethe potential and proper consideration of the locally broken charge symmetries near the cavity and at other interfaces in the simulation cell.

Figure 3 schematically indicates the different contributions to the electrostatic potential as a test charge is moved from the hard wall vacuum into a solute cavity near the hydrophobic length-scale transition size for SPC/E water. Ignoring the very small change at the wall-vapor interface, the first significant change $\Delta\phi_D$ is generated on crossing the LV interface due to the broken charge symmetry at this physical interface. For rigid models in a slab geometry, this can be shown to depend only on the average orientation of molecular dipole moments at the LV interface.[24,25]

Strictly speaking, there will also be an additional Bethe contribution ϕ_B to the potential change at the LV interface, proportional to the bulk LV density difference, as shown for the dashed red path in Figure 3. However, we know from the general argument above that this cannot contribute to the final Φ^{HW}, and it is conceptually simpler to imagine we are using a smeared water model with zero Bethe potential where only $\Delta\phi_D$ contribution appears, as depicted in the upper solid orange path.

The next and most physically relevant contribution $\Delta\phi_C$ for this path is generated by the locally broken charge symmetry near the cavity−water interface as the test charge moves into the cavity. We refer to $\Delta\phi_C$ as the cavity interface component. Thus, the final cavity potential has two components associated with broken symmetries at physical interfaces encountered along the path:

$$\Phi^{HW} = \Delta\phi_D + \Delta\phi_C \tag{3}$$

As would be expected, in the limit $R_C \to \infty$, the cavity potential $\Phi^{HW} \to 0$ since the interface approaches that of a hard wall or liquid−vapor interface. However, significant changes in $\Delta\phi_C$ occur at smaller R_C, particularly near the crossover radius, resulting from changes in the local hydrogen bond structure near the cavity, and this will be directly reflected in variations in Φ^{HW} as well as in $\Delta\phi_C$ itself.

These same conclusions follow from the dashed red path for general water models, since the Bethe contribution from the transit from the hard wall vacuum to bulk water indeed cancels identically with that from bulk water to the cavity vacuum, as indicated in Figure 3. This "two interface cancellation" picture has been stressed in previous work[4,6] and has been used to remove the Bethe contribution from estimates of the cavity potential. However, the $\Delta\phi_D$ contribution to Φ^{HW} from the distant HW interface remains in this picture, while solvation thermodynamics and effects of charging are dominated by the local structure around the cavity as reflected in $\Delta\phi_C$.

The various components of the cavity potential are reported in Table 1, and details pertaining to the calculation of the quantities in Table 1 are discussed in the SI. The most notable feature that emerges from the data in Table 1 is the consistent sign and magnitude of $\Delta\phi_C$ for both classical and DFT results; all cavity interface components are consistently negative and on the order of a tenth to a half of a volt. However, the magnitudes for $\Delta\phi_C$ obtained in SPC/E water are significantly larger than the TIP5P results, a direct consequence of the higher level of symmetry in the latter model and the concurrent solvation structure this manifests. This relative consistency for $\Delta\phi_C$ contrasts with the very different magnitudes and even signs for the Bethe potentials in different classical and quantum

dx.doi.org/10.1021/jz501067w | J. Phys. Chem. Lett. 2014, 5, 2767−2774

Table 1. Relevant Electrostatic Potential Differences in the System Considered in Figure 3

Model	R_C	$\Delta\phi_C$	ϕ_B	$\Delta\phi_D$	Φ^{HW}
SPC/E	2	−394	−850	+260	−147
	4	−522	−850	+260	−259
	6	−499	−850	+260	−251
TIP5P	2	−114	−200	+103	−9
	4	−136	−200	+103	−38
	6	−144	−200	+103	−42
BLYP	2	−372	+3870	+480	108
	4	−481	+3870	+480	−1
	6	−505	+3870	+480	−25
revPBE	2	−234	+3840	+480	246
	4	−401	+3840	+480	79
	6	−433	+3840	+480	47

The cavity interface component $\Delta\phi_C$, Bethe potential ϕ_B, the dipole component to the liquid−vapor surface potential $\Delta\phi_D$, and the net cavity potential Φ^{HW} are measured at the center of the cavity from the vapor, through the liquid−vapor interface, across the bulk, and into the cavity. All quantities are schematically depicted in Figure 3 and are reported in mV. The Bethe potential is calculated with respect to the location of the water oxygen site, as discussed in the text. It is important to note that for DFT calculations $\Delta\phi_C$ was estimated from direct use of eq 3 based on estimates of $\Delta\phi_D$ and Φ^{HW} (see SI). For the classical models, each component is computed independently and thus reflects all of the uncertainties contained therein.

models, but these fortunately play no role in most physical processes.

As a self-consistent check on the validity of our estimates for the cavity potential, we have also shown that $\Delta\phi_C$ can also be obtained using a *traceless* or Buckingham multipole expansion of eq 2, which must be valid for an observation point inside the cavity, as discussed above and further in the SI. In accord with previous findings,[7] we find that the local structure induced by the HS solute will produce significant contributions to $\Delta\phi_C$ through multipoles as high as the octupole moment for small values of R_C.

Surprisingly, the cavity interface components given by DFT models are in near quantitative agreement with the SPC/E model, although the structures of the two systems are quite different. We believe the quantitative consistency between these models is fortuitous. The structure obtained from DFT is consistent with TIP5P, and one might therefore expect a similar $\Delta\phi_C$. However, the DFT models implicitly include polarization at the interface, which increases the magnitude of $\Delta\phi_C$ relative to that of the classical TIP5P model.

Differences between the classical and quantum models arise because the intramolecular charge density of a single molecule in a rigid classical point charge model is trivially related to the nuclear structure of that molecule. However, this is not the case for quantum mechanics-based models, and the intramolecular charge density of a molecule will depend on its interactions with its surroundings through the electron density, leading to polarization and other many body configurational effects. This fact allows us to understand the differences that arise between the TIP5P and DFT models, which have similar solvation structures but yield different cavity potentials.

To illustrate this point, we resample the configurations generated with the classical SPC/E and TIP5P interaction potentials with DFT by performing wave function optimizations on the classical trajectories. Table 2 shows that Φ^{HW} for resampled TIP5P is in better agreement with the DFT values

Table 2. Electrostatic Potential Differences Obtained from DFT Resampling of Classically Generated Configurations

Model	R_C	$\Delta\phi_C$	$\Delta\phi_D$	Φ^{HW}
re-SPC/E	2	−228	+137	−191
	4	−474	+137	−337
re-TIP5P	2	−115	+70	−45
	4	−185	+70	−115

The cavity interface component $\Delta\phi_C$, the dipole component to the liquid−vapor surface potential $\Delta\phi_D$, and the net cavity potential Φ^{HW} are obtained from resampling of classical SPC/E and TIP5P configurations, indicated by the prefix "re-" when referring to the models. All quantities are reported in mV.

than those obtained from resampled SPC/E configurations. It should be pointed out that the value for Φ^{HW} under the resampled protocol is in good agreement with the value obtained by Beck (referred to as the "net potential") in similar fashion.[6] In contrast, $\Delta\phi_C$ values obtained from resampled SPC/E configurations are in better agreement with those from DFT simulations than that from TIP5P configurations. However, performing the resampling, and therefore including electronic effects, moves $\Delta\phi_C$ for TIP5P closer toward the DFT values while resampling increases the disparity between the SPC/E and DFT results, as expected from the similar solvation structure of the DFT and TIP5P models.

We conclude by emphasizing that the local molecular structure induced by a cavity is responsible for electrostatic potential changes most relevant for ion solvation thermodynamics through $\Delta\phi_C$. The detailed hydration structure around a hard solute near the crossover radius is dictated by the hydrogen bond network of water, and, as such, this structure depends sensitively on the interaction potentials used to model the aqueous solvent. In particular, whether or not lone pairs are explicitly modeled in classical point charge models, like the TIP5P and SPC/E models, significantly influences the solvation structure and the accompanying cavity interface component; models with explicit lone pairs are more symmetric with respect to interchange of lone pair and hydrogen positions. The TIP5P solvation structure is consistent with that of the quantum mechanics-based DFT simulations, and based on previous studies,[36,44−48] we posit that the unbiased DFT interaction potentials yield the physically correct solvent response to the hard solute.

The central focus of this work has been on the asymmetric local solvation structure around a cavity and how this structure influences the cavity potential Φ^{HW} through variations in the cavity interface component $\Delta\phi_C$. This electrostatic potential, and its dependence on the magnitude of a point charge placed at the center of the cavity in particular, is a key ingredient in understanding the solvation free energy of an ion, as well as in understanding fluctuations, dielectric response, and the decomposition of short- and long-range contributions to the electrostatic interaction energy. Here we have established that the Bethe potential can play no role in the solvation process. In future work we will focus on this process, and computation of ion hydration free energies in both classical and quantum models. This will provide a stringent test of the validity of both classical and quantum water models and of ion−water potentials.

dx.doi.org/10.1021/jz501067w | J. Phys. Chem. Lett. 2014, 5, 2767−2774

METHODS

Systems with buffering liquid−vapor interfaces contain 340 water molecules and a hard sphere excluded volume in the center of the simulation cell modeled in a slab configuration. Cell dimensions are 20 × 20 × 70 Å^3 for the classical point charge (SPC/E[16] and TIP5P[17]) and 20 × 20 × 50 Å^3 for DFT interaction potentials. The hard sphere excluded volume with radius R_C interacts with the water oxygens (distance to center of the simulation cell R_C) only through an external potential centered in the middle of the simulation cell:

$$V(r) = 1 - \tanh\left(\frac{r - R_C}{0.02}\right) \quad (4)$$

All DFT simulations were performed using the CP2K simulation suite.[49] The energies and forces were computed for the ab initio MD within the QUICKSTEP module,[49] which contains an accurate and efficient implementation of DFT that employs dual basis sets of Gaussian-type orbitals (molopt-DZV2P) and plane waves (expanded to 400 Ry) for the electron density.[50] Only the valence electrons were considered explicitly, and the core electrons were represented using Goedecker−Teter−Hutter pseudopotentials.[51] Two different DFT functionals, the Becke exchange and correlation due to Lee, Yang, and Parr (BLYP),[52,53] as well as the revised Perdew, Burke, and Ernzerhof (revPBE)[54,55] were simulated using a dispersion correction, introduced by Grimme, D1 and D3, for BLYP and revPBE, respectively.[56−58] Periodic images were screened by using a two-dimensional wavelet Poisson solver.[59] A Nosé−Hoover thermostat chain[60] of length 3 was coupled to every molecule and maintained a temperature of 300 K, and an integration time step of 0.5 fs was utilized. The BLYP trajectories were started from an equilibrated SPC/E initial configuration. Two trajectories were spawned for the 2 and 4 Å solute sizes. A total of ∼40 ps was used as a production run with the first 7 ps of each trajectory discarded. For the 6 Å sphere a single trajectory was spawned yielding roughly 20 ps with the first 7 ps discarded for equilibration. The revPBE runs were started from the equilibrated BLYP trajectories. Production runs of 25−30 ps for each sphere size was used to analyze the data. The classical Molecular dynamics simulations used the standard three-dimensional Ewald method.[61]

Additional classical molecular dynamics simulations of cavity solvation in bulk (in the absence of a buffering liquid−vapor interface) were performed with a modified version of DL_POLY v2.18[62] in the isothermal−isobaric (NPT) ensemble for solute sizes in the range $0 < R_C < 10$ Å. Results obtained using this approach are virtually identical to those obtained in the presence of a liquid−vapor interface, however, fewer water molecules can be used, permitting more efficient exploration of the solute size range of interest. A temperature and pressure of 300 K and 1 atm were maintained using a Berendsen thermostat and barostat, respectively.[63] The evaluation of electrostatic interactions employed the Ewald summation method.[61]

ASSOCIATED CONTENT

Supporting Information

Nonuniform densities around solutes, description of the calculation of the Bethe potential in classical and quantum systems, multipole analysis of the cavity potential, a discussion of cavity potential statistics, and orientational preferences of classical models around all solutes studied. This material is available free of charge via the Internet http://pubs.acs.org.

AUTHOR INFORMATION

Corresponding Authors

*E-mail: rremsing@umd.edu.
*E-mail: chris.mundy@pnnl.gov.
*E-mail: jdw@umd.edu.

Present Address

‖(R.C.R.) Department of Chemical and Biomolecular Engineering, University of Pennsylvania, Philadelphia, Pennsylvania 19104.

Notes

The authors declare no competing financial interest.

ACKNOWLEDGMENTS

JDW and RCR are financially supported by the National Science Foundation (Grants CHE0848574 and CHE1300993). CJM and GKS are financially supported by the U.S. Department of Energy's (DOE) Office of Basic Energy Sciences, Division of Chemical Sciences, Geosciences and Biosciences. Pacific Northwest National Laboratory (PNNL) is operated for the Department of Energy by Battelle. MDB is grateful for the support of the Linus Pauling Distinguished Postdoctoral Fellowship Program at PNNL. We acknowledge illuminating discussions and sharing of ideas and preprints with Dr. Shawn M. Kathmann, Dr. Bernhard Sellner, and Prof. Tom Beck. The DFT simulations used resources provided by the National Energy Research Scientific Computing Center, which is supported by the Office of Science of the U.S. Department of Energy under Contract No. DE-AC02-05CH11231. Additional computing resources were generously allocated by PNNL's Institutional Computing program.

REFERENCES

(1) Bardhan, J. P.; Jungwirth, P.; Makowski, L. Affine-Response Model of Molecular Solvation of Ions: Accurate Predictions of Asymmetric Charging Free Energies. *J. Chem. Phys.* **2012**, *137*, 124101.
(2) Ashbaugh, H. S. Convergence of Molecular and Macroscopic Continuum Descriptions of Ion Hydration. *J. Phys. Chem. B* **2000**, *104*, 7235−7238.
(3) Song, X.; Chandler, D.; Marcus, R. A. Gaussian Field Model of Dielectric Solvation Dynamics. *J. Phys. Chem.* **1996**, *100*, 11954−11959.
(4) Harder, E.; Roux, B. On the Origin of the Electrostatic Potential Difference at a Liquid−Vacuum Interface. *J. Chem. Phys.* **2008**, *129*, 234706.
(5) Rajamani, S.; Ghosh, T.; Garde, S. Size Dependent Ion Hydration, Its Asymmetry, and Convergence to Macroscopic Behavior. *J. Chem. Phys.* **2004**, *120*, 4457.
(6) Beck, T. L. The Influence of Water Interfacial Potentials on Ion Hydration in Bulk Water and near Interfaces. *Chem. Phys. Lett.* **2013**, *561−562*, 1−13.
(7) Horváth, L.; Beu, T.; Manghi, M.; Palmeri, J. The Vapor−Liquid Interface Potential of (Multi)Polar Fluids and Its Influence on Ion Solvation. *J. Chem. Phys.* **2013**, *138*, 154702.
(8) Born, M. Volumes and Hydration Warmth of Ions. *Z. Phys.* **1920**, *1*, 45−48.
(9) Leung, K.; Rempe, S. B.; von Lilienfeld, O. A. Ab Initio Molecular Dynamics Calculations of Ion Hydration Free Energies. *J. Chem. Phys.* **2009**, *130*, 204507.
(10) Leung, K.; Marsman, M. Energies of Ions in Water and Nanopores within Density Functional Theory. *J. Chem. Phys.* **2007**, *127*, 154722.

(11) Hummer, G.; Pratt, L. R.; García, A. E. Free Energy of Ionic Hydration. *J. Phys. Chem.* **1996**, *100*, 1206−1215.
(12) Beck, T. L. Hydration Free Energies by Energetic Partitioning of the Potential Distribution Theorem. *J. Stat. Phys.* **2011**, *145*, 335−354.
(13) Shi, Y.; Beck, T. L. Length Scales and Interfacial Potentials in Ion Hydration. *J. Chem. Phys.* **2013**, *139*, 044504.
(14) Hummer, G.; Pratt, L. R.; García, A. E. Molecular Theories and Simulation of Ions and Polar Molecules in Water. *J. Phys. Chem. A* **1998**, *102*, 7885−7895.
(15) Agmon, N. Liquid Water: From Symmetry Distortions to Diffusive Motion. *Acc. Chem. Res.* **2012**, *45*, 63−73.
(16) Berendsen, H. J. C.; Grigera, J. R.; Straatsma, T. P. The Missing Term in Effective Pair Potentials. *J. Phys. Chem.* **1987**, *91*, 6269−6271.
(17) Mahoney, M.; Jorgensen, W. A Five-Site Model for Liquid Water and the Reproduction of the Density Anomaly by Rigid, Nonpolarizable Potential Functions. *J. Chem. Phys.* **2000**, *112*, 8910−8922.
(18) Remsing, R. C.; Rodgers, J. M.; Weeks, J. D. Deconstructing Classical Water Models at Interfaces and in Bulk. *J. Stat. Phys.* **2011**, *145*, 313−334.
(19) Remsing, R. C.; Weeks, J. D. Dissecting Hydrophobic Hydration and Association. *J. Phys. Chem. B* **2013**, *117*, 15479−15491.
(20) Zangwill, A. *Modern Electrodynamics*; Cambridge University Press: Cambridge, UK, 2013.
(21) Harris, F. E. In *Hartee−Fock Studies of Electronic Structures of Crystalline Solids in Theoretical Chemistry: Advances and Perspectives*; Eyring, H., Henderson, D., Eds.; Academic Press: New York/London, 1975, Vol. *1*.
(22) Kholopov, E. V. Mean Potential of Bethe in the Classical Problem of Calculating Bulk Electrostatic Potentials in Crystals. *Phys. Status Solidi B* **2006**, *243*, 1165−1181.
(23) Kathmann, S. M.; Kuo, I.-F. W.; Mundy, C. J.; Schenter, G. K. Understanding the Surface Potential of Water. *J. Phys. Chem. B* **2011**, *115*, 4369−4377.
(24) Wilson, M. A.; Pohorille, A.; Pratt, L. R. Comment on "Study on the Liquid−Vapor Interface of Water. I. Simulation Results of Thermodynamics Properties and Orientational Structure". *J. Chem. Phys.* **1989**, *90*, 5211−5213.
(25) Pratt, L. R. Contact Potentials of Solution Interfaces: Phase Equilibrium and Interfacial Electric Fields. *J. Phys. Chem.* **1992**, *96*, 25−33.
(26) Hunenberger, P.; Reif, M. *Single−Ion Solvation: Experimental and Theoretical Approaches to Elusive Thermodynamic Properties*; Theoretical and Computational Chemistry; RCS: Cambridge, UK, 2011; Vol. *3*.
(27) Lin, Y.-L.; Aleksandrov, A.; Simonson, T.; Roux, B. An Overview of Electrostatic Free Energy Computations for Solutions and Proteins. *J. Chem. Theory. Comput.* **2014**, *10*, 2690−2709.
(28) Grossman, J. C.; Schwegler, E.; Galli, G. Quantum and Classical Molecular Dynamics Simulations of Hydrophobic Hydration Structure around Small Solutes. *J. Phys. Chem. B* **2004**, *108*, 15865−15872.
(29) Jedlovszsky, P.; Predota, M.; Nezbeda, I. Hydration of Apolar Solutes of Varying Size: A Systematic Study. *Mol. Phys.* **2006**, *104*, 2465−2476.
(30) Berne, B. J.; Weeks, J. D.; Zhou, R. Dewetting and Hyrophobic Interactions in Physical and Biological Systems. *Annu. Rev. Phys. Chem.* **2009**, *60*, 85−103.
(31) Hummer, G.; Garde, S.; García, A. E.; Paulaitis, M. E.; Pratt, L. R. Hydrophobic Effects on a Molecular Scale. *J. Phys. Chem. B* **1998**, *102*, 10469−10482.
(32) Rajamani, S.; Truskett, T. M.; Garde, S. Hydrophobic Hydration from Small to Large Lengthscales: Understanding and Manipulating the Crossover. *Proc. Natl. Acad. Sci. U. S. A.* **2005**, *102*, 9475−9480.
(33) Lum, K.; Chandler, D.; Weeks, J. D. Hydrophobicity at Small and Large Length Scales. *J. Phys. Chem. B* **1999**, *103*, 4570−4577.
(34) Chandler, D. Interfaces and the Driving Force of Hydrophobic Assembly. *Nature* **2005**, *437*, 640−647.
(35) Stillinger, F. H. Structure in Aqueous Solutions of Nonpolar Solutes from the Standpoint of Scaled-Particle Theory. *J. Solution Chem.* **1973**, *2*, 141−158.
(36) Baer, M. D.; Stern, A. C.; Levin, Y.; Tobias, D. J.; Mundy, C. J. Electrochemical Surface Potential Due to Classical Point Charge Models Drives Anion Adsorption to the Air−Water Interface. *J. Phys. Chem. Lett.* **2012**, *3*, 1565−1570.
(37) Vorobyov, I.; Allen, T. W. The Electrostatics of Solvent and Membrane Interfaces and the Role of Electronic Polarizability. *J. Chem. Phys.* **2010**, *132*, 185101.
(38) Hummer, G.; Pratt, L. R.; García, A. E.; Berne, B. J.; Rick, S. W. Electrostatic Potentials and Free Energies of Solvation of Polar and Charged Molecules. *J. Phys. Chem. B* **1997**, *101*, 3017−3020.
(39) Hummer, G.; Pratt, L. R.; García, A. E.; Garde, S.; Berne, B. J.; Rick, S. W. Reply to Comment on "Electrostatic Potentials and Free Energies of Solvation of Polar and Charged Molecules". *J. Phys. Chem. B* **1998**, *102*, 3841−3843.
(40) Ashbaugh, H. S.; Sakane, S.; Wood, R. H. Reply to Comment on "Electrostatic Potentials and Free Energies of Solvation of Polar and Charged Molecules". *J. Phys. Chem. B* **1998**, *102*, 3844−3845.
(41) Aqvist, J.; Hansson, T. Analysis of Electrostatic Potential Truncation Schemes in Simulations of Polar Solvents. *J. Phys. Chem. B* **1998**, *102*, 3837−3840.
(42) Kastenholz, M. A.; Hünenberger, P. H. Computation of Methodology-Independent Ionic Solvation Free Energies from Molecular Simulations. I. The Electrostatic Potential in Molecular Liquids. *J. Chem. Phys.* **2006**, *124*, 124106.
(43) Kastenholz, M. A.; Hünenberger, P. H. Computation of Methodology-Independent Ionic Solvation Free Energies from Molecular Simulations. II. The Hydration Free Energy of the Sodium Cation. *J. Chem. Phys.* **2006**, *124*, 224501.
(44) Baer, M. D.; Mundy, C. J. Toward an Understanding of the Specific Ion Effect Using Density Functional Theory. *J. Phys. Chem. Lett.* **2011**, *2*, 1088−1093.
(45) Baer, M. D.; Pham, V.-T.; Fulton, J. L.; Schenter, G. K.; Balasubramanian, M.; Mundy, C. J. Is Iodate a Strongly Hydrated Cation? *J. Phys. Chem. Lett.* **2011**, *2*, 2650−2654.
(46) Fulton, J. L.; Schenter, G. K.; Baer, M. D.; Mundy, C. J.; Dang, L. X.; Balasubramanian, M. Probing the Hydration Structure of Polarizable Halides: A Multiedge XAFS and Molecular Dynamics Study of the Iodide Anion. *J. Phys. Chem. B* **2010**, *114*, 12926−12937.
(47) Fulton, J. L.; Bylaska, E. J.; Bogatko, S.; Balasubramanian, M.; Cauet, E.; Schenter, G. K.; Weare, J. H. Near-Quantitative Agreement of Model-Free DFT-MD Predictions with XAFS Observations of the Hydration Structure of Highly Charged Transition-Metal Ions. *J. Phys. Chem. Lett.* **2012**, *3*, 2588−2593.
(48) Baer, M. D.; Mundy, C. J. An Ab Initio Approach to Understanding the Specific Ion Effect. *Faraday Discuss.* **2013**, *160*, 89−101.
(49) VandeVondele, J.; Krack, M.; Mohamed, F.; Parrinello, M.; Chassaing, T.; Hutter, J. QUICKSTEP: Fast and Accurate Density Functional Calculations Using a Mixed Gaussian and Plane Waves Approach. *Comput. Phys. Commun.* **2005**, *167*, 103−128.
(50) VandeVondele, J.; Hutter, J. Gaussian Basis Sets for Accurate Calculations on Molecular Systems in Gas and Condensed Phases. *J. Chem. Phys.* **2007**, *127*, 114105.
(51) Goedecker, S.; Teter, M.; Hutter, J. Separable Dual-Space Gaussian Pseudopotentials. *Phys. Rev. B* **1996**, *54*, 1703−1710.
(52) Becke, A. D. Density-Functional Exchange-Energy Approximation with Correct Asymptotic Behavior. *Phys. Rev. A* **1988**, *38*, 3098−3100.
(53) Lee, C.; Yang, W.; Parr, R. G. Development of the Colle−Salvetti Correlation-Energy Formula into a Functional of the Electron Density. *Phys. Rev. B* **1988**, *37*, 785−789.
(54) Perdew, J.; Burke, K.; Ernzerhof, M. Generalized Gradient Approximation Made Simple. *Phys. Rev. Lett.* **1996**, *77*, 3865−3868.
(55) Zhang, Y.; Yang, W. Comment on "Generalized Gradient Approximation Made Simple". *Phys. Rev. Lett.* **1998**, *80*, 890.

(56) Grimme, S. Accurate Description of van der Waals Complexes by Density Functional Theory Including Empirical Corrections. *J. Comput. Chem.* **2004**, *25*, 1463−1473.
(57) Grimme, S. Semiempirical GGA-Type Density Functional Constructed with Long-Range Dispersion Correction. *J. Comput. Chem.* **2006**, *27*, 1787−1799.
(58) Grimme, S.; Antony, J.; Ehrlich, S.; Krieg, H. A Consistent and Accurate Ab Initio Parametrization of Density Functional Dispersion Correction (DFT-D) for the 94 Elements H−Pu. *J. Chem. Phys.* **2010**, *132*.
(59) Genovese, L.; Deutsch, T.; Neelov, A.; Goedecker, S.; Beylkin, G. Efficient Solution of Poisson's Equation with Free Boundary Conditions. *J. Chem. Phys.* **2006**, *125*.
(60) Martyna, G. J.; Klein, M. L.; Tuckerman, M. E. Nose−Hoover Chains - The Canonical Ensemble via Continous Dynamics. *J. Chem. Phys.* **1992**, *97*, 2635−2643.
(61) Allen, M. P.; Tildesley, D. J. *Computer Simulation of Liquids*; Oxford: New York, 1987.
(62) Smith, W.; Yong, C.; Rodger, P. DL_POLY: Application to Molecular Simulation. *Mol. Simul.* **2002**, *28*, 385−471.
(63) Berendsen, H. J. C.; Postma, J. P. M.; van Gunsteren, W. F.; DiNiola, A.; Haak, J. R. Molecular Dynamics with Coupling to an External Bath. *J. Chem. Phys.* **1984**, *81*, 3684.